Distinct Functional Connectivity Mode during Viewing Natural Scenes Revealed by Principal Component Analysis

Murat Demirtaş[1,2], Adrian Ponce-Alvarez[2], Matthieu Gilson[2], Patric Hagmann[4],Dante Mantini[5,6], Viviana Betti[7], Gian Luca Romani[8], Karl Friston[9], Maurizio Corbetta[10], Gustavo Deco[2,3]

[1]N3 Division, Department of Psychiatry, Yale University, 40 Temple Street, New Haven, 06511, Connecticut, United States

[2]Center for Brain and Cognition, Computational Neuroscience Group, Department of Information and Communication Technologies, Universitat Pompeu Fabra, Roc Boronat 138, Barcelona, 08018, Spain

[3]Institució Catalana de la Recerca i Estudis Avançats (ICREA), Universitat Pompeu Fabra, Passeig Lluís Companys 23, Barcelona, 08010, Spain

[4]Department of Radiology, Lausanne University Hospital and University of Lausanne (CHUV-UNIL), Rue du Bugnon 46, 1011 Lausanne, Switzerland.

[5]Research Center for Motor Control and Neuroplasticity, KU Leuven, Tervuursevest 101, 3001 Leuven, Belgium.

[6]Department of Neurorehabilitation, IRCCS San Camillo Hospital Foundation, via Alberoni 70, 30126 Venice Lido, Italy.

[7]Department of Psychology, Sapienza University of Rome, via dei Marsi 78, 00185 Rome; Fondazione Santa Lucia and Istituto Di Ricovero e Cura a Carattere Scientifico, 00142, Rome, Italy.

[8]Institute for Advanced Biomedical Technologies, “G. d’Annunzio” University of Chieti-Pescara, 66100, Chieti, Italy.

[9]Wellcome Trust Centre for Neuroimaging, Institute of Neurology, University College London, 12 Queen Square, London WC1N 3BG, United Kingdom.

[10]Departments of Neurology, Radiology, Anatomy of Neurobiology, School of Medicine, Washington University, St. Louis, St Louis, USA

Corresponding author:

Murat Demirtaş, Yale University, 40 Temple Street, New Haven, 06511, Connecticut, United States. murat.demirtas@yale.edu

Abstract

A fundamental question in systems neuroscience is how spontaneous activity at rest is reorganized during task performance. Recent studies suggest a strong relationship between resting and task FC. Furthermore, the relationship between resting and task FC has been shown to reflect individual differences. Particularly, various studies have demonstrated that the FC has higher reliability and provides enhanced detection of individual differences while viewing natural scenes. Although the large-scale organization of FC during rest and movie-viewing conditions have been well studied in relation to individual variations, the re-organization of FC during viewing natural scenes have not been studied in depth. In this study, we used principal component analysis on FC during rest and movie-viewing condition to characterize the dimensionality of FC patterns across conditions and subjects. We found that the variations in FC patterns related to viewing natural scenes can be explained by a single component, which enables identification of the task over subjects with 100% accuracy. We showed that the FC mode associated to viewing natural scenes better reflects individual variations. Furthermore, we investigated the signatures of movie-viewing-specific functional modes in dynamic FC based on phase-locking values between brain regions. We found that the movie-specific functional mode is persistent across time; suggesting the emergence of a stable processing mode. To explain the reorganization of whole-brain FC through the changes in local dynamics, we appeal to a large-scale computational model. This modelling suggested that the reorganization of whole-brain FC is associated to the interaction between frontal-parietal and frontal-temporal activation patterns.

Introduction

Neural dynamics underwrite information processing at multiple spatiotemporal scales. The neural correlates of information processing at a local scale have been widely studied. However, the integration of information in whole-brain level is also crucial for understanding brain function (Baars, 1993; Tononi, 2004). Long-range synchronization of oscillatory activity has been proposed as dynamical mechanism for mediating the interaction between brain areas in a task-dependent manner (Engel et al., 2001; Fries, 2005). Recent studies showed that neuronal synchronization mediates neuronal communication in large-scale cortical networks during task performance (Betti et al., 2013) and resting state (de Pasquale et al., 2010).

Resting state functional connectivity (rs-FC) is a powerful technique to characterize large-scale organization of brain activity based on the temporal correlations between blood oxygen level-dependent (BOLD) signals (Biswal et al., 1995). Rs-FC patterns have been shown to provide 'fingerprints' for the functional brain organization of individuals (Finn et al., 2015). Furthermore, recent studies showed strong relationship between the FC during resting state and task performance (Betti et al., 2013; Cole et al., 2014, 2016; Rosenberg et al., 2015). The relationship between resting state and task FC has been shown to reflect individual differences (Tavor et al., 2016). In particular, experimental paradigms such as viewing natural scenes (i.e. movie watching) are of interest due to their ecological validity (Betti et al., 2013). Several studies found that FC has higher reliability and provides enhanced detection of individual differences while viewing natural scenes (Kim et al., 2017; Vanderwal et al., 2015, 2017). However, the features underlying the enhanced reliability of FC are not clear given that the large-scale organization of FC is very similar during rest and viewing natural scenes. Theoretical studies have proposed that entropy of the cortical activity space is reduced during task (Ponce-Alvarez et al., 2015). Therefore, the functional reorganization during viewing natural scenes is expected to reflect not only individual subject-specific variations but also task-specific variations. Nevertheless, the task-dependent reorganization of FC during viewing natural scenes and its relationship to individual subject-specific variations are poorly understood.

Understanding the organization of whole-brain FC during distinct conditions is challenging because of enormous dimensionality, which increases quadratically with the number of brain regions. Principal component analysis (PCA) is widely known and intuitive mathematical procedure to characterize the dimensionality of data. PCA transforms a set of observations into orthogonal components and allows characterizing the relationship between these orthogonal components and the projections of individual observations. PCA and associated techniques have been used to characterize resting-state fluctuations (Carbonell et al., 2011), whole-brain connectivity dynamics (Allen et al., 2012) and disease-related rs-FC states (Craddock et al., 2009). In this paper, we used PCA to investigate the dimensionality of FC during rest and movie-viewing condition. Based on the projections of individual subjects and sessions on principal components, we identified FC-states specific to natural viewing condition. Then, we

studied the consistency of this principal component across sessions, subjects, and under different preprocessing approaches.

Another important question related to the task-dependent reorganization of FC is whether alterations in grand-average FC (over the whole session) reflect a persistent (temporally stable) functional state or they reflect the emergence of various functional states fluctuating over time (Gonzalez-Castillo et al., 2015). To answer this question, we extended our analysis beyond grand-average FC states and investigated the temporal fluctuations in FC states based on the dynamics of phase-coupling among brain regions.

Although empirical findings provide insights on the task-dependent reorganization of whole-brain FC, these results may not offer a mechanistic understanding. We therefore adopted a mechanistic approach for task-dependent reorganization of whole-brain FC using large-scale by physically plausible modelling framework. We constraint the long-range interactions between brain regions by diffusion weight imaging-derived (DWI) structural connectivity, and studied the alterations in local dynamics of each brain regions during natural viewing conditions.

Results

Principal component analysis reveals distinctive FC mode during movie watching condition

The grand average FC during resting state and movie exhibited similar patterns (r = 0.8, p-value < 0.0001) (Figure 1A). However, the similarity across FCs of individual subjects was substantially higher under the same condition (resting state r = 0.46 ± 0.06; movie r = 0.49 ± 0.06) than across conditions (r = 0.40 ± 0.07). To characterize the variations in FC during rest-state and movie viewing conditions, we performed principal component analysis (PCA) across FCs of individual subjects (Figure 1B-C).

We concatenated FCs of 21 individuals during 2 separate sessions of resting state and movie watching conditions and then employed PCA. We found that the first principal component (PC-1) explaining 25.8% of the variance (Figure 2A) reflected the dominant FC pattern that were conserved over conditions. The projections of PC-1 were significantly correlated with global signal standard deviations of individual subjects/session (r = 0.99, p-value < 0.0001) (Figure 2J). This result suggested that the principal mode of variation in FC reflects the global signal variance and associated overall synchronization levels. However, the second principal component (PC-2) (Figure 2C) explaining 7.2% of the variance clearly distinguished the movie condition from resting state. Based on the projections of two principal components (i.e. 2-dimensional projections of subject/session data on principal components), we found that movie-specific PC-2 separates the two conditions with 100% accuracy (Figure 2D).

Previous studies have shown restricted subject movements and increased arousal while watching natural scenes (Vanderwal et al., 2015). Therefore, the movie-specific PC may also reflect the contributions of artefactual signal changes. To rule out possible artefactual contributions, we repeated the analyses after regressing out the global signal (Figure 2E-H). We found that after global signal regression (GSR) the first principal component (PC-1) explaining 9.69% of the variance reflected movie-specific variations in FC. The projections of PC-1 separated two conditions with 100% accuracy (Figure 2H). Furthermore, the topologies of movie-specific component modes were highly consistent with and without GSR (r = 0.81, p-value < 0.0001). These results showed that the movie-specific variations in FC patterns can be explained by a single dimension.

Movie-specific FC variations are consistent across sessions and they reflect individual variations better than non-specific principal components

We repeated the PCA (with and without GSR) using 2 sessions separately. For both sessions we found the movie-specific and non-specific components without GSR (Figure 3A-B) and with GSR (Figure 3C-D). Without GSR, PC-1 (global signal component) of session 1 and session 2 was significantly correlated (r = 0.75, p-value < 0.0001). However, the similarity between movie-specific PC-2 of session 1 and session 2 was substantially higher than that of PC-1 (r = 0.83,

p < 0.0001). Similarly, with GSR, we found higher similarity between session 1 and session 2 for movie-specific PC-1 (r = 0.82, p-value < 0.0001) than for non-specific PC-2 (r = 0.54, p-value < 0.0001). These results show that the movie-specific principal component is highly consistent across sessions.

To investigate the individual variations associated to each principal component, we compared the PC projections across sessions. We found that the projections of movie-specific components were highly consistent across sessions (without GSR r = 0.92, p-value < 0.0001; with GSR r = 0.93, p-value < 0.0001), and the correlations were substantially higher than those of non-specific components (without GSR r = 0.76, p-value < 0.0001; with GSR r = 0.52, p-value < 0.0001). These results show that the FC topography related to movie-watching conditions reflects individual variations better than that related to resting condition.

Movie-specific FC patterns are temporally stable

We investigated whether the movie-specific FC patterns are temporally stable in time or whether they emerge as a consequence of the fluctuations in FC (i.e. collection of single or multiple transient states). We constructed dynamic FC (dFC) based on the time-dependent fluctuations in phase-locking values (PLVs) between brain regions. First, we band-pass filtered the BOLD time-series in 0.04-0.07Hz narrow-band. After employing Hilbert transform, we calculated the PLVs at each time point using instantaneous phases of each brain region (Figure 4A). Then, we calculated the correlation between the instantaneous PLVs and average PLVs of resting state and movie sessions. To avoid any session-specific bias, we calculated the correlations between average PLVs of resting state and movie from session 1 and instantaneous PLVs of session 2 (and vice versa). We also repeated the PCA on average PLV matrices for session 1 and session 2 (Figure 4C, F). We found that the principal components based on PLVs exhibit movie condition specificity for both sessions. Furthermore, movie-specific PC of PLVs were highly correlated with that of Pearson correlation based FC (r = 0.88, p-value < 0.0001).

For resting state sessions, the correlations between PLVs and average PLVs of movie sessions were significantly lower than that for resting state sessions across time points (Wilcoxon signed-rank test p-value < 0.0001, for both session 1 and session 2). For movie sessions, the correlations between PLVs and average PLVs of movie sessions were significantly higher than that for resting state sessions across time points (Wilcoxon signed-rank test p-value < 0.0001, for both session 1 and session 2) (Figure 4D-E). The results were the same when the analyses were repeated using movie-specific and non-specific principal components instead of average PLVs (Supplementary Figure 1). In addition, we constructed the average dFC across subjects and estimated the correlation between the average PLVs at each time-point and average PLVs of resting-state and movie sessions. We found that for both resting state and movie sessions, the PLVs at each time-point exhibited higher correlations with grand-average PLVs of matching

condition (Supplementary Figure 1). We further employed PCA over the PLV fluctuations concatenated across sessions for each subject. The trajectories of the principle components revealed emergence of movie-specific FC as a distinct mode for most of the subjects (Supplementary Figure 2). Nevertheless, we did not find task-specific components for PLVs concatenated across all subjects and all sessions. These results suggest that the movie-specific FC pattern emerges as a temporally stable mode during movie watching sessions, although the time-resolved FC states is difficult to estimate.

Large-scale computational modelling of the regional dynamics underlying movie-watching FC

We used a large-scale computational model to characterize the alterations in regional dynamics associated to the movie-watching condition. We used Hopf normal model to characterize the BOLD activity of each region (Deco et al., 2017). The regions were coupled to each other via DWI-derived structural connectivity scaled by a global coupling parameter (Figure 5A). The dynamics of each region were governed by local bifurcation parameter (a). The local bifurcation parameters (a) reflects whether an individual region is dominantly in a noise-driven regime ($a < 0$), oscillatory regime ($a > 0$), or alternates between the two regimes ($a \sim 0$) (Figure 5A). We estimated the optimal global coupling and local bifurcation parameters of each subject/session by maximizing the similarity (i.e. Pearson correlation) between empirical and model FCs using gradient-descent optimization. There was no significant difference in the model fit for resting-state ($r = 0.518 \pm 0.057$) and movie sessions ($r = 0.497 \pm 0.045$) ($T = 1.256$, p-value = 0.219, permutation t-test).

To characterize the overall topology underlying each condition, first we estimated the optimal global coupling parameter (g) and optimal bifurcation parameters (a) for resting state and movie watching condition based on the similarity between average empirical and model FC. At rest, the average optimal bifurcation parameters were low in parietal and temporal regions, whereas they were higher in occipital and frontal regions (Figure 5B). For movie condition, the bifurcation parameters were increased in parietal and temporal regions and decreased in anterior cingulate, lateral prefrontal cortices and in supramarginal gyrus (Figure 5C). There was no significant difference between the mean optimal bifurcation parameters of rest and movie conditions (Figure 5D).

To quantify the group differences, we compared regional optimal bifurcation parameters of resting state and movie sessions (Figure 6A). We found no significant differences in global coupling parameters between rest and movie conditions (Figure 6B). In movie condition, the local bifurcation parameters were significantly decreased towards negative values in bilateral caudal anterior and posterior cingulate, right supramarginal gyrus, and left post- and para-central cortices (Figure 6D). In contrast, the bifurcation parameters were significantly increased in bilateral orbital frontal cortex, right lateral orbital frontal cortex, right middle rostral frontal

cortex, right superior parietal cortex, right fusiform gyrus, and left frontal pole and left medial temporal cortex (Figure 6D).

Finally, we repeated the PCA on optimal bifurcation parameters across subjects and conditions (Figure 6E-G). The first principal component (PC-1) explaining 41.77% of the variation and the second principal component (PC-2) explaining 10.25% of the variation were both significantly correlated with the contrast between average bifurcation parameters of movie and resting-state sessions (PC-1 $r = 0.38$, p-value = 0.002; PC-2 $r = 0.73$, p-value < 0.0001). The first principal component (PC-1) exhibited a strong positive peak in precuneus and isthmus of cingulate, slightly higher values in medial frontal and temporal regions, which is very similar to default mode network (DMN) topography (Figure 6E). The second principal component (PC-2) showed higher values in temporal and frontal regions (Figure 6F). Furthermore, the second principal component (PC-2) exhibited movie specificity (Figure 6G). This result shows that the alterations in regional dynamics in the movie-condition reflect at enhanced influence of frontal-temporal brain regions on whole-brain dynamics.

Discussion

We characterized the reorganization of FC during natural viewing condition compared to resting state. Using principal component analysis, we found that the alterations in FC during natural viewing condition can be explained along a single dimension or mode of variation (i.e. a condition-specific pattern of connectivity that captures the variations across subjects). The projections of the FCs of each subject on the movie-specific principal component provided a clear separation between conditions with classification accuracy of 100%.

FC signatures of viewing natural scenes

The movie-specific FC topology exhibited enhanced connectivity between occipital-temporal regions and frontal-parietal regions (Supplementary Figure 3). This result can be interpreted as enhanced communication between sensory and association regions during natural viewing condition. Previous studies reported that the subjects show decreased head movements and higher arousal while natural viewing condition (Vanderwal et al., 2015). Therefore, the exceptionally high classification power can also reflect systematic artifacts. To rule of this possibility we repeated the analysis after global signal regression (GSR), separate sessions, bandpass filtered signals, and phase-locking values. We found that the results are invariant to different preprocessing approaches. Furthermore, the movie-specific FC mode was highly consistent before and after GSR, and across sessions. The correlations between movie-specific components across sessions were higher than those for non-specific components. These findings confirmed previous studies showing the enhanced reliability and individual subject detection during natural viewing conditions (Kim et al., 2017; Vanderwal et al., 2017). In addition, we showed that the enhanced reliability and individual subject detection during natural viewing conditions are driven by task-specific reorganization of FC, which is distinct from the resting-state related individual variations.

Before GSR, the first principal component reflected the overall synchronization in FC (as well as global signal variance). This was an expected result, since the global signal was consistently reported as explaining the large amount of variation in BOLD signals (Carbonell et al., 2011). However, our results showed that the global signal component is not related to the movie condition. After GSR the global synchronization component disappeared, whereas the movie-specific component remained intact. It is important to note that the global signal component reflects the common FC topology across subjects and it was strongly correlated across sessions. The high correlations between the projections of global signal components across sessions suggest that the global signal component also explains individual variations. In other words, the variations and similarities across subjects during resting-state are mostly driven by the differences in global signal variance. However, in this study, it cannot be known to what extend the global signal-related component and individual variations reflect neural, hemodynamic and/or artefactual differences. The relationship between global signal

fluctuations and whole-brain synchronization is essential to understand individual subject variations at resting-state.

Stable task-specific FC patterns in dynamic FC

We also investigated how movie-specific FC topography relates to the dynamic FC. We used Hilbert transform on narrowband filtered time-series and characterized dynamic FC based on phase-locking values across time. We found that the movie-specific principal components also appear in FC and average PLVs of the narrowband filtered time-series. Then, we calculated the similarity between grand-average PLVs of resting state and movie during one session and the PLV fluctuations during the other session. We found that for movie sessions the PLV of each time point was persistently more similar to the average PLVs of the movie sessions than to those of the resting state sessions. In contrast, for resting sessions the PLV of each time point was more similar to the resting state FC than to the movie FC. Overall, these results showed that during natural viewing condition the FC is persistently reorganized into its associated mode. One limitation of this approach is the substantial observation noise of instantaneous PLVs in conjunction with limited variance explained by the PCs, which leads to very low correlations between instantaneous PLVs. The stability of task-related FC patterns is important for the assumptions behind large-scale computational modeling. Our results suggest that whole-brain FC (at the time-scale of BOLD signals) is persistently reconfigured into a distinct mode rather than an epiphenomenon reflecting activation of several transient states.

Computational modeling of task-specific alterations

Although variations related to the natural viewing condition can be explained in a single dimension, it is very difficult interpret a whole-brain connectivity pattern. We proposed a computational model to link the alterations in local dynamics to reorganization of whole-brain FC. We used Hopf normal model to characterize BOLD signals. The motivation behind using this model was that noise-driven and oscillatory dynamics can be modeled using a single parameter (local bifurcation parameter). When the local bifurcation parameter of a particular region is negative, the region exhibits noise-driven dynamics. For positive bifurcation parameter values, the region exhibits sustained oscillations. Therefore, higher parameters values of a region in the model indicate that the region has higher influence on its connected regions. The model revealed significant decreases in bifurcation parameters particularly in cingulate cortex (anterior and posterior cingulate) and in supramarginal gyrus. In contrast, the bifurcation parameters significantly increased in lateral prefrontal cortex, medial temporal cortex and superior parietal regions. These results showed that during movie condition, the influence of frontal, temporal and parietal association regions on the whole-brain FC is enhanced. Nevertheless, it is important to note that the model describes the BOLD signals in the associated low-frequency narrow-band. Therefore, higher values of the bifurcation parameters

can also be interpreted as the contribution of low-frequency fluctuations in the regions is enhanced since hemodynamic responses act as a low-pass filter. Furthermore, BOLD signals are known to have negative relationship with the neural activity in middle frequency ranges (Schölvinck et al., 2013). Therefore, the increased/decreased local bifurcation parameters should be interpreted only in relation to low-frequency fluctuations.

Since the empirical data provided a clear separation of rest and movie conditions, we also employed PCA on the bifurcation parameters of the model. The first PC mode showed a typical pattern associated to the default mode network (DMN), in which the high values were observed in isthmus cingulate, precuneus, medial frontal and temporal cortices. The second principal component mode, characterized by higher bifurcation parameter values in temporal and frontal regions, showed movie-specificity. These results suggested that the variations in bifurcation parameters in frontal-parietal and frontal-temporal networks have exclusive contributions to the organization of whole-brain FC during movie-viewing condition. Furthermore, we found that the projections of the first and second principal components on movie sessions were negatively correlated (spearman rank r = -0.496, p-value= 0.02). Therefore, the variations across both task-specific and DMN-like activation patterns, and the antagonistic relationship between these patterns are associated to task-related organization of FC. Nevertheless, based on these results, it is not possible to draw conclusions on the causal mechanisms that drive the relationship between DMN and task-related networks. The results may indicate that several regions of DMN (particularly precuneus) having a role in mediating the switch between distinct functional states, which is consistent with previous studies showing that precuneus dynamically binds to distinct functional networks (Utevsky et al., 2014). An alternative explanation may involve the variations of arousal and vigilance levels. This explanation is consistent with a selective neuromodulatory enabling of intrinsic synaptic connections by ascending modulatory neurotransmitter systems (e.g., noradrenaline). This is particularly relevant in light of the systematic changes in the local bifurcation parameter that showed regionally-specific and condition-sensitive effects in our modelling analyses.

Limitations

One limitation of our modeling results is that the model relies on DWI-derived SC, which has limited performance on detecting interhemispheric connections, individual variations, and also directions of the connections. In addition, the changes in directed effective connectivity may also play role in defining the reorganization of FC during task (Gilson et al., 2017). We re-analyzed the alterations in EC (Gilson et al., 2017) based on our current findings: the PCA analysis of EC exhibited a better and clearer separation between resting-state and movie sessions than FC (Supplementary Figure 4). Furthermore, the movie-specific principal component of EC revealed enhanced connectivity from frontal regions towards parietal and occipital brain regions, and from occipital and temporal regions toward parietal and frontal

regions (Supplementary Figure 3). Therefore, during natural viewing condition lower sensory regions in occipital and temporal regions project to frontal and parietal higher-order association regions, and that this pattern is completed as a recurrent loop by the frontal regions projecting towards parietal regions and parietal regions projecting towards temporal and occipital regions. These results are consistent with the alterations that we found in the local dynamics (i.e. under fixed-connectivity assumption) such that frontal and parietal regions play crucial role in re-organization of FC during task. In contrast, the model based on local dynamics cannot resolve the alterations in sensory regions. Effective connectivity – as assessed using dynamic causal modelling studies of the resting state – again point to a modulation of regional excitability by different components of the default mode. For example, previous studies revealed that the influence of the SN (salience network) and DAN (dorsal attention network) on the DMN (default mode network) regions is inhibitory; whereas the DMN exerted an excitatory influence on the SN and DAN regions (Zhou et al., 2018). Therefore, we speculate that the alterations in higher-order association regions are better captured by the local dynamics because these regions contribute to whole-brain organization through strong bidirectional connections across the cortex, whereas the influence of sensory regions is dominantly unidirectional.

Conclusion and future directions

Current experimental paradigms are optimal to study task-dependent changes in BOLD signals, but these are not optimal to study task-dependent re-organization of whole-brain FC. Naturalistic condition, such as movie watching, that is comparable to the resting-state, may have important implications on understanding the dynamic organization of whole-brain activity. Here, we proposed a novel approach to link task-dependent functional organization and dynamic functional connectivity. Nevertheless, it may not be possible to exploit the full potential of dynamic organization of the brain through natural viewing paradigms. The major limitation of this approach is that the natural viewing condition is a trivial task. Future studies may explore other natural experimental paradigms that involve more challenging conditions such as problem solving, navigation, social interactions, task engagement during present distractors. We speculate that sophisticated natural tasks that require enhanced cognitive control may reveal richer dynamical manifestation of functional reorganization. For example, certain challenging tasks may show a better picture of dynamic reorganization of the whole-brain such as consolidation of particular functional states in time (i.e. slow adaptation) and/or emergence of observable transient functional states (i.e. multistability).

Materials and Methods

Study design

The fMRI imaging data used in this paper have been described in details elsewhere (Betti et al., 2013; Mantini et al., 2012). Twenty-four right-handed young, healthy volunteers (15 females, 20–31 years old) participated in the study. They were informed about the experimental procedures, which were approved by the Ethics Committee of the Chieti University, and signed a written informed consent. The study included a resting state and a natural vision condition. In the resting state, participants fixated a red target with a diameter of 0.3 visual degrees on a black screen. In the natural-vision condition, subjects watched (and listened) to 30 minutes of the movie “The Good, the Bad and the Ugly” in a window of 24x10.2 visual degrees. Visual stimuli were projected on a translucent screen using an LCD projector, and viewed by the participants through a mirror tilted by 45 degrees. Auditory stimuli were delivered using MR-compatible headphones.

Data acquisition

Functional imaging was performed with a 3T MR scanner (Achieva; Philips Medical Systems, Best, The Netherlands) at the Institute for Advanced Biomedical Technologies in Chieti, Italy. The functional images were obtained using T2*-weighted echo-planar images (EPI) with BOLD contrast using SENSE imaging. EPIs comprised of 32 axial slices acquired in ascending order and covering the entire brain (32 slices, 230 x 230 in-plane matrix, TR/TE=2000/35, flip angle = 90°, voxel size=2.875×2.875×3.5 mm3). For each subject, 2 and 3 scanning runs of 10 minutes duration were acquired for resting state and natural vision, respectively. Each run included 5 dummy volumes – allowing the MRI signal to reach steady state, and an additional 300 functional volumes that were used for analysis. Eye position was monitored during scanning using a pupil-corneal reflection system at 120 Hz (Iscan, Burlington, MA, USA). A three-dimensional high-resolution T1-weighted image, for anatomical reference, was acquired using an MP-RAGE sequence (TR/TE=8.1/3.7, voxel size=0.938x0.938x1 mm3) at the end of the scanning session.

Data preprocessing

Data preprocessing was performed using SPM5 (Wellcome Department of Cognitive Neurology, London, UK) running under MATLAB (The Mathworks, Natick, MA). The preprocessing steps involved the following: (1) correction for slice-timing differences (2) correction of head-motion across functional images, (3) coregistration of the anatomical image and the mean functional image, and (4) spatial normalization of all images to a standard stereotaxic space (Montreal Neurological Institute, MNI) with a voxel size of 3×3×3 mm3. Furthermore, the BOLD time series in MNI space were subjected to spatial independent component analysis (ICA) for the identification and removal of artifacts related to blood pulsation, head movement and instrumental spikes (Smith et al., 2010). This BOLD artifact

411 removal procedure was performed by means of the GIFT toolbox (Medical Image Analysis Lab,
412 University of New Mexico). No global signal regression or spatial smoothing was applied.
413 For each recording session (subject and run), we extracted the mean BOLD time series from
414 the 66 regions of interest (ROIs) of the brain atlas (Hagmann et al., 2008)(see Supplementary
415 Table 1). 2 subjects were excluded due to signal dropout and 1 subject was excluded due to
416 substantial spikes in the time-series.
417
418 **Anatomical Connectivity**
419 Anatomical connectivity was estimated from Diffusion Spectrum Imaging (DSI) data collected
420 in five healthy right-handed male participants (Hagmann et al., 2008; Honey et al., 2009). The
421 grey matter was first parcellated into 66 ROIs, using the same low-resolution atlas used for the
422 FC analysis. For each subject, we performed white matter tractography between pairs of
423 cortical areas to estimate a neuroanatomical connectivity matrix. The coupling weights between
424 two brain areas were quantified using the fiber tract density, and were proportional to a
425 normalized number of detected tracts. The structural matrix (SC) was then obtained by
426 averaging the matrices over subjects.
427
428 **Principal component analysis**
429 For all subjects and sessions (i.e. 21 subjects, 2 resting state and 2 movie sessions) the
430 functional connectivity matrices were constructed based on Pearson correlation coefficient
431 between all pairs of ROIs.
432 The upper triangular parts of FC (i.e. $66(66-1)/2$ connections) matrices were concatenated
433 across subjects/sessions (21x4 session/subjects) leading to the feature matrix with dimensions
434 2145 x 84 (number of connections x number of sessions/subjects). Then, principal component
435 analysis was applied to the resulting feature matrix. The analyses were repeated for 1000
436 surrogates time-series with preserved power-spectrum based on each session/subject. The
437 dimensionality of the data was characterized by explained variance of the principal components
438 that are larger than those of the surrogates.
439 To quantify the consistency of principal components, we repeated the analysis using 2 separate
440 sessions. For both sessions, the feature matrices comprised the concatenated upper triangular
441 FC matrices of 1 resting state session and 1 movie session (i.e. 2145 x 42 matrices). The
442 consistency across sessions was quantified as Pearson correlation coefficients of the
443 components and the projection of components between sessions.
444 Since during natural viewing condition the individuals are shown to have restricted movements
445 and increase arousal (Vanderwal et al., 2015), the differences in FC can be substantially
446 affected by underlying artifacts. For this reason, we repeated all the analyses after regressing
447 out global signal from the time-series of each ROI.
448
449 **Dynamic functional connectivity**
450 Preprocessed time series were band-pass filtered in 0.04-0.07Hz range in order to reduce the

effects of low-frequency drift and high-frequency noise (Glerean et al., 2012). Then, Hilbert transform was used for the assessment of dynamic functional connectivity (Demirtaş et al., 2016; Glerean et al., 2012). The Hilbert transform, $S(t) = A\cos(\varphi(t))$ of the preprocessed BOLD time series broke the signal down to an analytical signal *S(t)* with an instantaneous phase *φ(t)* and amplitude *A*. For each time point *t*, the difference $\Delta\varphi_{ij}(t)$ between the phases of the respective ROIs was calculated, where *i* and *j* are the indices of each ROI. The phase differences were adjusted between 0 and *π* such that:

$$\Delta\varphi_{ij}(t) = \begin{matrix} |\varphi_i(t) - \varphi_j(t)|, & if\ |\varphi_i(t) - \varphi_j(t)| \leq \pi \\ 2\pi - |\varphi_i(t) - \varphi_j(t)|, & otherwise \end{matrix} \quad (1)$$

Then, the phase-locking values (PLVs), $PLV_{ij}(t)$ were constructed using the phase differences normalized between 0 and 1, thereby representing perfect anti-synchronization and perfect synchronization respectively, such that: $PLV_{ij}(t) = 1 - \Delta\varphi_{ij}(t)/\pi$.

We computed the grand-average PLVs for each session (i.e. resting state and movie watching). Then, for each subject, we calculated the similarity (Pearson correlation coefficient) between grand-average PLVs and time-resolved PLVs. In brief, for each subject two quantities were estimated and compared as a function of time: the correlation between instantaneous PLVs and grand-average PLVs for resting state and that for movie condition. To avoid the bias caused by shared variability within each session, we calculated the grand-average PLVs of one session, and then the similarities were calculated for the other session. Therefore, the analysis was performed twice: the grand-average PLVs of session 1 projected to the PLVs of session 2 and the grand-average PLVs of session 2 projected to the PLVs of session 1. To provide a better illustration for the magnitudes of correlations, we performed a same analysis averaging the time-resolved PLVs across subjects (Supplementary Figure 1).

The principal component analysis was repeated for band-pass filtered time-series and average PLVs. Since the PLVs were much more sensitive to global synchronization levels, we subtracted the mean from each average PLV matrix. We also repeated the time-resolved analysis using movie-specific and non-specific principal component instead of grand-average PLVs. After identifying the principal component whose projections distinguish the resting condition from movie condition, we re-projected each component on the instantaneous PLVs using Pearson correlation coefficient (Supplementary Figure 1). We also performed PCA over the concatenated time courses (i.e. 2 resting state and 2 movie sessions) of individual subject PLVs. The trajectories of the first 2 principal components were plotted to illustrate the switch between resting and movie watching conditions (Supplementary Figure 2).

Computational modeling

We modeled the whole-brain rs-fMRI BOLD signals using 66 nodes. Each node was coupled with each other via DWI-derived structural connectivity (SC) matrix. We described the local dynamics of each individual node using normal form of a supercritical Hopf bifurcation (Deco

et al., 2017). The advantage of this model is that it allows transitions between asynchronous noise activity and oscillations. Where ω is the intrinsic frequency of each node, a is the local bifurcation parameter, η is additive Gaussian noise with standard deviation β, the temporal evolution of the activity, z, in node j is given in complex domain as:

$$\frac{dz_j}{dt} = [a_j + i\omega_j - |z_j^2|] + \beta\eta_j(t) \quad (2)$$

and,

$$z_j = \rho_j e^{i\theta_j} = x_j + iy_j \quad (3)$$

This system shows a supercritical bifurcation at $a_j = 0$. Being specific, if a_j is smaller than 0, the local dynamics has a stable fixed point at $z_j = 0$, and for a_j values larger than 0, there exists a stable limit cycle oscillation with a frequency $f = \omega/2\pi$. Finally, the whole-brain dynamics is described by the following coupled equations:

$$\frac{dx_j}{dt} = [a_j - x_j^2 - y_j^2]x_j - \omega_j y_j + g\sum_i C_{ij}(x_i - x_j) + \beta\eta_{xj}(t) \quad (4)$$

$$\frac{dy_j}{dt} = [a_j - x_j^2 - y_j^2]y_j + \omega_j x_j + g\sum_i C_{ij}(y_i - y_j) + \beta\eta_{yj}(t) \quad (5)$$

Where C_{ij} is the Structural Connectivity (SC) between nodes i and j, g is the global coupling factor, and the standard deviation of Gaussian noise, $\beta = 0.02$. The natural frequency (f) of each region was taken as the peak frequency in the given narrowband of the corresponding region in the empirical time-series.

Following a similar approach previously employed on biophysically-based computational model (Deco et al., 2014), we analytically estimated the model FC using linearization of the system around a stable fix point. Where $\delta\mathbf{u} = \{\delta x_1 \dots \delta x_{66}, \delta y_1 \dots \delta y_{66}\}$ represents the Taylor expansion of the system, **A** is the Jacobian matrix, and $\varepsilon(t)$ is the noise term, the fluctuations around the fix point can be described as:

$$\frac{d\delta\mathbf{u}}{dt} = \mathbf{A}\delta\mathbf{u} + \varepsilon(t) \quad (6)$$

Where the deterministic parts of right-hand side of equations 4 and 5 are described by $-F_j$ and $-G_j$, respectively, the Jacobian matrix of the system evaluated at the fixed point $\hat{x_j}, \hat{y_j}, j \in \{1 \dots 66\}$ can be constructed as:

$$\mathbf{A} = \begin{bmatrix} \frac{\partial F_1}{\partial x_1} & \cdots & \frac{\partial F_1}{\partial x_N} & \frac{\partial F_1}{\partial y_1} & \cdots & \frac{\partial F_1}{\partial y_N} \\ \vdots & \ddots & \vdots & \vdots & \ddots & \vdots \\ \frac{\partial F_N}{\partial x_1} & \cdots & \frac{\partial F_N}{\partial x_N} & \frac{\partial F_N}{\partial y_1} & \cdots & \frac{\partial F_N}{\partial y_N} \\ \frac{\partial G_j}{\partial x_1} & \cdots & \frac{\partial G_1}{\partial x_N} & \frac{\partial G_1}{\partial y_1} & \cdots & \frac{\partial G_N}{\partial y_1} \\ \vdots & \ddots & \vdots & \vdots & \ddots & \vdots \\ \frac{\partial G_N}{\partial x_1} & \cdots & \frac{\partial G_N}{\partial x_N} & \frac{\partial G_1}{\partial y_N} & \cdots & \frac{\partial G_N}{\partial y_N} \end{bmatrix}$$

Where $i, j \in \{1 \dots 66\}$, each element of matrix **A** can be calculated as:

$$\frac{\partial F_j}{\partial x_j} = \frac{\partial G_j}{\partial y_j} = a - g \sum\nolimits_k C_{jk} \quad (7)$$

$$\frac{\partial F_j}{\partial x_l} = \frac{\partial G_j}{\partial y_l} = g C_{jl} \quad (8)$$

$$\frac{\partial F_j}{\partial y_j} = -\omega_0 \quad (9)$$

$$\frac{\partial G_j}{\partial y_j} = \omega_0 \quad (10)$$

$$\frac{\partial F_j}{\partial x_l} = \frac{\partial G_j}{\partial y_l} = 0 \quad (11)$$

Where **Q** is the noise covariance matrix, the covariance matrix of the system **P** can be estimated by solving Lyapunov equation:

$$\mathbf{AP} + \mathbf{PA^T} = -\mathbf{Q} \quad (12)$$

Finally, the model correlation matric (FC) can be extracted from the covariance matrix as:

$$mFC_{ij} = \frac{P_{ij}}{\sqrt{P_{ii} P_{jj}}}, i, j \in \{1 \dots 66\} \quad (13)$$

We estimated the model optimal parameters a and g by maximizing the similarity between model FC (equation 13) and empirical FC using gradient descent optimization. To avoid the solutions reflecting a local minimum, for each subject/session we estimated the best solution after repeating the optimization with 100 random initial conditions. The similarity between model FC and empirical FC was quantified as Pearson correlation coefficient. For each subject, the empirical functional connectivity was calculated as the average FC across the corresponding conditions (i.e. resting state or movie sessions) of the corresponding subject.

The group comparisons for resting state versus movie sessions (optimal bifurcation parameters and global coupling parameter) were done using permutation t-test (5000 permutations). For

549 optimal bifurcation parameters, the p-values were corrected using FDR approach with
550 Benjamini&Hochberg algorithm if necessary (Hochberg and Benjamini, 1990).
551
552 **Acknowledges**
553
554 We thank Alan Anticevic, John Murray, Markus Helmer and Joshua Burt for the insightful
555 discussions and their comments during the preparation of this paper.
556
557 **References**
558 Allen, E.A., Damaraju, E., Plis, S.M., Erhardt, E.B., Eichele, T., Calhoun, V.D., 2012. Tracking
559 Whole-Brain Connectivity Dynamics in the Resting State. Cereb. Cortex bhs352.
560 https://doi.org/10.1093/cercor/bhs352
561 Baars, B.J., 1993. A cognitive theory of consciousness., A cognitive theory of consciousness.
562 Cambridge University Press, New York, NY, US.
563 Betti, V., Della Penna, S., de Pasquale, F., Mantini, D., Marzetti, L., Romani, G.L., Corbetta,
564 M., 2013. Natural scenes viewing alters the dynamics of functional connectivity in the human
565 brain. Neuron 79, 782–797. https://doi.org/10.1016/j.neuron.2013.06.022
566 Biswal, B., Yetkin, F.Z., Haughton, V.M., Hyde, J.S., 1995. Functional connectivity in the motor
567 cortex of resting human brain using echo-planar MRI. Magn Reson Med 34, 537–541.
568 Carbonell, F., Bellec, P., Shmuel, A., 2011. Global and System-Specific Resting-State fMRI
569 Fluctuations Are Uncorrelated: Principal Component Analysis Reveals Anti-Correlated
570 Networks. Brain Connect 1, 496–510. https://doi.org/10.1089/brain.2011.0065
571 Cole, M.W., Bassett, D.S., Power, J.D., Braver, T.S., Petersen, S.E., 2014. Intrinsic and Task-
572 Evoked Network Architectures of the Human Brain. Neuron 83, 238–251.
573 https://doi.org/10.1016/j.neuron.2014.05.014
574 Cole, M.W., Ito, T., Bassett, D.S., Schultz, D.H., 2016. Activity flow over resting-state networks
575 shapes cognitive task activations. Nat Neurosci 19, 1718–1726.
576 https://doi.org/10.1038/nn.4406
577 Craddock, R.C., Holtzheimer, P.E., Hu, X.P., Mayberg, H.S., 2009. Disease state prediction
578 from resting state functional connectivity. Magn. Reson. Med. 62, 1619–1628.
579 https://doi.org/10.1002/mrm.22159
580 de Pasquale, F., Della Penna, S., Snyder, A.Z., Lewis, C., Mantini, D., Marzetti, L., Belardinelli,
581 P., Ciancetta, L., Pizzella, V., Romani, G.L., Corbetta, M., 2010. Temporal dynamics of
582 spontaneous MEG activity in brain networks. Proceedings of the National Academy of Sciences
583 107, 6040–6045. https://doi.org/10.1073/pnas.0913863107
584 Deco, G., Kringelbach, M.L., Jirsa, V.K., Ritter, P., 2017. The dynamics of resting fluctuations
585 in the brain: metastability and its dynamical cortical core. Scientific Reports 7.
586 https://doi.org/10.1038/s41598-017-03073-5
587 Deco, G., Ponce-Alvarez, A., Hagmann, P., Romani, G.L., Mantini, D., Corbetta, M., 2014. How
588 Local Excitation-Inhibition Ratio Impacts the Whole Brain Dynamics. The Journal of

589 Neuroscience 34, 7886–7898. https://doi.org/10.1523/JNEUROSCI.5068-13.2014
590 Demirtaş, M., Tornador, C., Falcón, C., López-Solà, M., Hernández-Ribas, R., Pujol, J.,
591 Menchón, J.M., Ritter, P., Cardoner, N., Soriano-Mas, C., Deco, G., 2016. Dynamic functional
592 connectivity reveals altered variability in functional connectivity among patients with major
593 depressive disorder. Hum. Brain Mapp. 37, 2918–2930. https://doi.org/10.1002/hbm.23215
594 Engel, A.K., Fries, P., Singer, W., 2001. Dynamic predictions: Oscillations and synchrony in
595 top–down processing. Nature Reviews Neuroscience 2, 704–716.
596 https://doi.org/10.1038/35094565
597 Finn, E.S., Shen, X., Scheinost, D., Rosenberg, M.D., Huang, J., Chun, M.M., Papademetris,
598 X., Constable, T.R., 2015. Functional connectome fingerprinting: identifying individuals using
599 patterns of brain connectivity 18, 1664–1671. https://doi.org/10.1038/nn.4135
600 Fries, P., 2005. A mechanism for cognitive dynamics: neuronal communication through
601 neuronal coherence. Trends in Cognitive Sciences 9, 474–480.
602 https://doi.org/10.1016/j.tics.2005.08.011
603 Gilson, M., Deco, G., Friston, K.J., Hagmann, P., Mantini, D., Betti, V., Romani, G.L., Corbetta,
604 M., 2017. Effective connectivity inferred from fMRI transition dynamics during movie viewing
605 points to a balanced reconfiguration of cortical interactions. NeuroImage.
606 https://doi.org/10.1016/j.neuroimage.2017.09.061
607 Glerean, E., Salmi, J., Lahnakoski, J.M., Jaaskelainen, I.P., Sams, M., 2012. Functional
608 Magnetic Resonance Imaging Phase Synchronization as a Measure of Dynamic Functional
609 Connectivity. Brain Connect 2, 91–101. https://doi.org/10.1089/brain.2011.0068
610 Gonzalez-Castillo, J., Hoy, C.W., Handwerker, D.A., Robinson, M.E., Buchanan, L.C., Saad,
611 Z.S., Bandettini, P.A., 2015. Tracking ongoing cognition in individuals using brief, whole-brain
612 functional connectivity patterns. Proceedings of the National Academy of Sciences 112, 8762–
613 8767. https://doi.org/10.1073/pnas.1501242112
614 Hagmann, P., Cammoun, L., Gigandet, X., Meuli, R., Honey, C.J., Wedeen, V.J., Sporns, O.,
615 2008. Mapping the Structural Core of Human Cerebral Cortex. PLoS Biol 6, e159.
616 https://doi.org/10.1371/journal.pbio.0060159
617 Hochberg, Y., Benjamini, Y., 1990. More powerful procedures for multiple significance testing.
618 Statist. Med. 9, 811–818. https://doi.org/10.1002/sim.4780090710
619 Honey, C.J., Sporns, O., Cammoun, L., Gigandet, X., Thiran, J.P., Meuli, R., Hagmann, P.,
620 2009. Predicting human resting-state functional connectivity from structural connectivity. PNAS
621 106, 2035–2040. https://doi.org/10.1073/pnas.0811168106
622 Kim, D., Kay, K., Shulman, G.L., Corbetta, M., 2017. A New Modular Brain Organization of the
623 BOLD Signal during Natural Vision. Cerebral Cortex 1–17.
624 https://doi.org/10.1093/cercor/bhx175
625 Mantini, D., Corbetta, M., Romani, G.L., Orban, G.A., Vanduffel, W., 2012. Data-driven analysis
626 of analogous brain networks in monkeys and humans during natural vision. NeuroImage 63,
627 1107–1118. https://doi.org/10.1016/j.neuroimage.2012.08.042
628 Ponce-Alvarez, A., He, B.J., Hagmann, P., Deco, G., 2015. Task-Driven Activity Reduces the

629 Cortical Activity Space of the Brain: Experiment and Whole-Brain Modeling. PLOS
630 Computational Biology 11, e1004445. https://doi.org/10.1371/journal.pcbi.1004445
631 Rosenberg, M.D., Finn, E.S., Scheinost, D., Papademetris, X., Shen, X., Constable, R.T.,
632 Chun, M.M., 2015. A neuromarker of sustained attention from whole-brain functional
633 connectivity. Nature Neuroscience 19, 165–171. https://doi.org/10.1038/nn.4179
634 Schölvinck, M.L., Leopold, D.A., Brookes, M.J., Khader, P.H., 2013. The contribution of
635 electrophysiology to functional connectivity mapping. NeuroImage, Mapping the Connectome
636 80, 297–306. https://doi.org/10.1016/j.neuroimage.2013.04.010
637 Smith, J.F., Pillai, A., Chen, K., Horwitz, B., 2010. Identification and validation of effective
638 connectivity networks in functional magnetic resonance imaging using switching linear dynamic
639 systems. NeuroImage 52, 1027–1040. https://doi.org/10.1016/j.neuroimage.2009.11.081
640 Tavor, I., Jones, O.P., Mars, R.B., Smith, S.M., Behrens, T.E., Jbabdi, S., 2016. Task-free MRI
641 predicts individual differences in brain activity during task performance. Science 352, 216–220.
642 https://doi.org/10.1126/science.aad8127
643 Tononi, G., 2004. An information integration theory of consciousness. BMC Neuroscience 5,
644 42. https://doi.org/10.1186/1471-2202-5-42
645 Utevsky, A.V., Smith, D.V., Huettel, S.A., 2014. Precuneus Is a Functional Core of the Default-
646 Mode Network. J Neurosci 34, 932–940. https://doi.org/10.1523/JNEUROSCI.4227-13.2014
647 Vanderwal, T., Eilbott, J., Finn, E.S., Craddock, R.C., Turnbull, A., Castellanos, F.X., 2017.
648 Individual differences in functional connectivity during naturalistic viewing conditions.
649 NeuroImage 157, 521–530. https://doi.org/10.1016/j.neuroimage.2017.06.027
650 Vanderwal, T., Kelly, C., Eilbott, J., Mayes, L.C., Castellanos, F.X., 2015. Inscapes : A movie
651 paradigm to improve compliance in functional magnetic resonance imaging. NeuroImage 122,
652 222–232. https://doi.org/10.1016/j.neuroimage.2015.07.069
653 Zhou, Y., Friston, K.J., Zeidman, P., Chen, J., Li, S., Razi, A., 2018. The Hierarchical
654 Organization of the Default, Dorsal Attention and Salience Networks in Adolescents and Young
655 Adults. Cerebral Cortex 28, 726–737. https://doi.org/10.1093/cercor/bhx307
656
657

Figures and captions

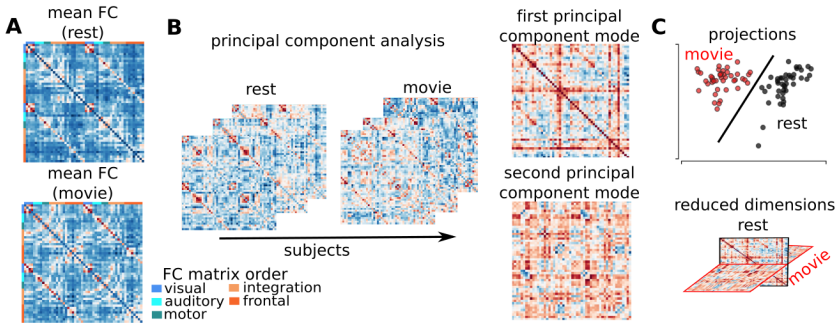

Figure 1. Conceptual overview. **A** Mean FC across subjects during resting state (top) and movie (bottom) sessions. For convenience the matrices were ordered by pre-defined networks involving visual, auditory, motor, integration and frontal regions. **B-C** Overview of principal component analysis (PCA). The FCs of the subjects at each session were concatenated into a single feature matrix. Then PCs of the feature matrix was calculated **(B)**. Note that the (vectorized) FC features pertain to correlations over the number of regions squared. However, the principal components of these FC features can be reorganized into a connectivity matrix that has the same size as the number of connections – as shown on the right (of panel B).The projections of each subject/session of the first two principal components were plotted against each other **(C)**. The second principal component projections revealed a clear distinction between rest and movie sessions (top) leading to representation of FC variations in two dimensions (bottom).

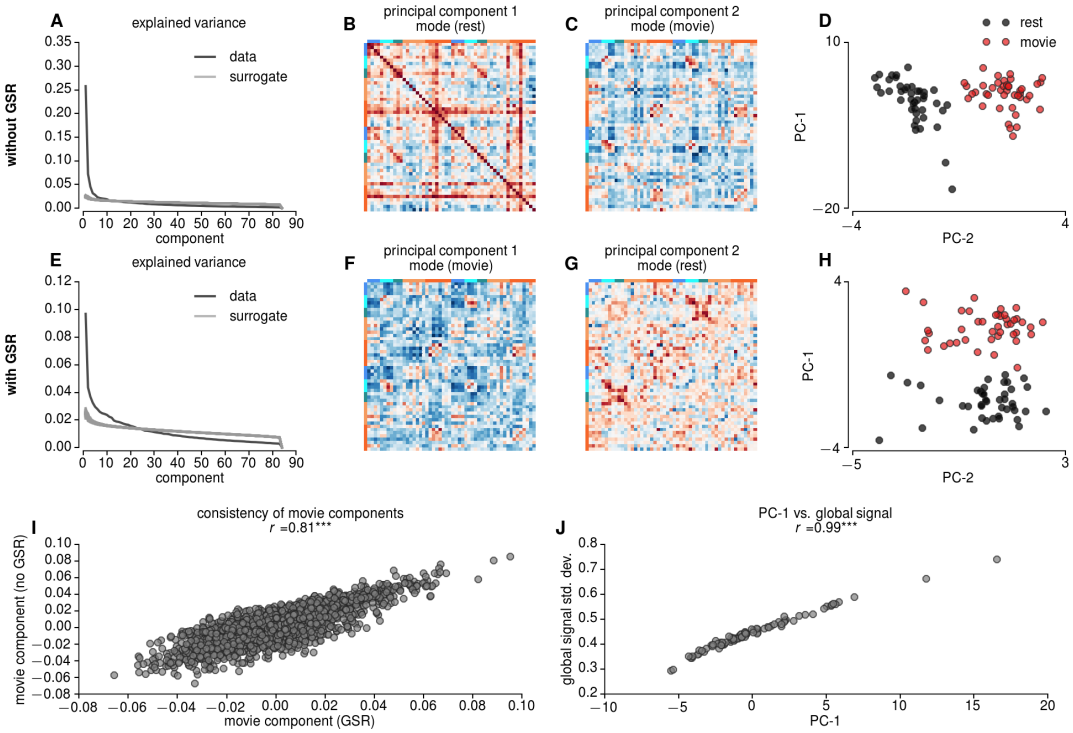

Figure 2. Principal component analysis of FC based on 2 resting state and 2 movie sessions concatenated across 21 subjects. **A-D.** Results without global signal regression (GSR). **A** Explained variance by each PC (black) and random surrogates (gray) without GSR. Compared to 1000 random surrogates the dimensionality of FCs without GSR is 13. The first PC **(B)** explains 25.8% of the variation, whereas second PC **(C)** explains 7.2% of the variation. The projections of first two PCs reveals that the second component is specific to movie sessions **(D)**. The first PC of the FCs without GSR reflects global signal standard deviation **(J)**. **E-H.** Results with global signal regression (GSR). **E** Explained variance by each PC (black) and random surrogates (gray) with GSR. Compared to random surrogates the dimensionality of FCs with GSR is 22. The first PC, which is specific to movie sessions explains 9.69% of the variation **(F)**. The movie-specific components with and without GSR is highly consistent. *** p-value < 0.0001.

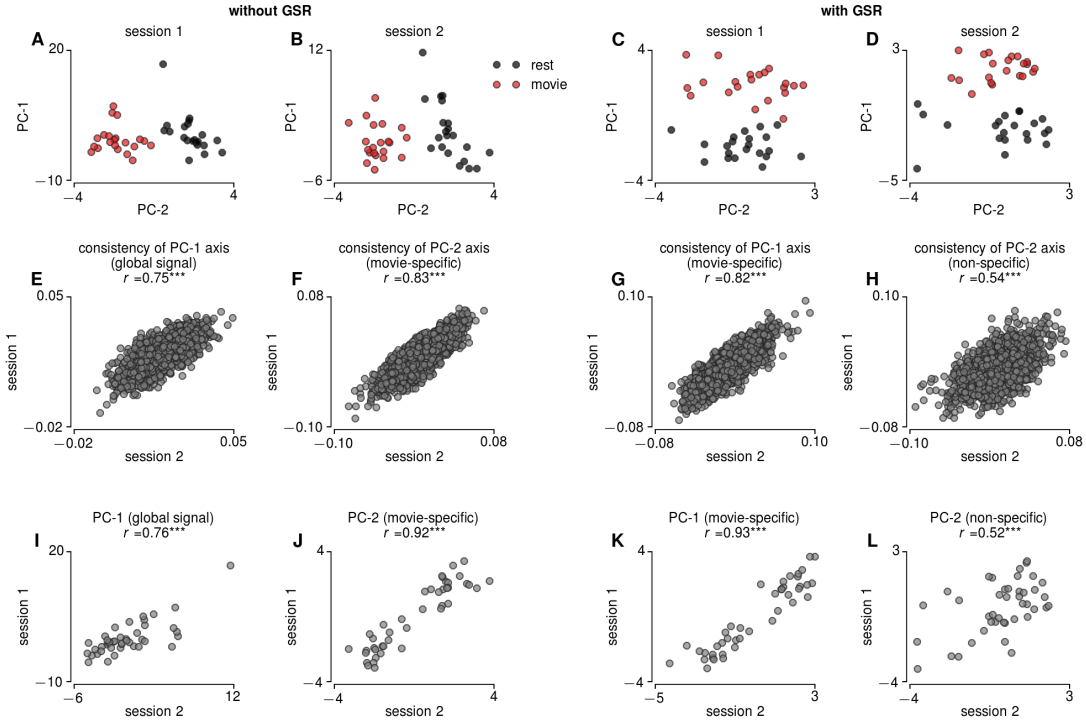

Figure 3. The consistency of principal components across sessions. The second PC is specific to movie session in both session 1 **(A)** and session 2 **(B)** without GSR, whereas the first PC is movie-specific in session 1 **(C)** and session 2 **(D)** with GSR. The consistency of the movie-specific component (**F** without GSR; **G** with GSR) is substantially higher than that of the non-specific components (**E** without GSR; **H** with GSR). Similarly, the consistency of the projections for movie-specific component (**J** without GSR; **K** with GSR) is substantially higher than that of the non-specific components (**I** without GSR; **L** with GSR). *** p-value < 0.0001.

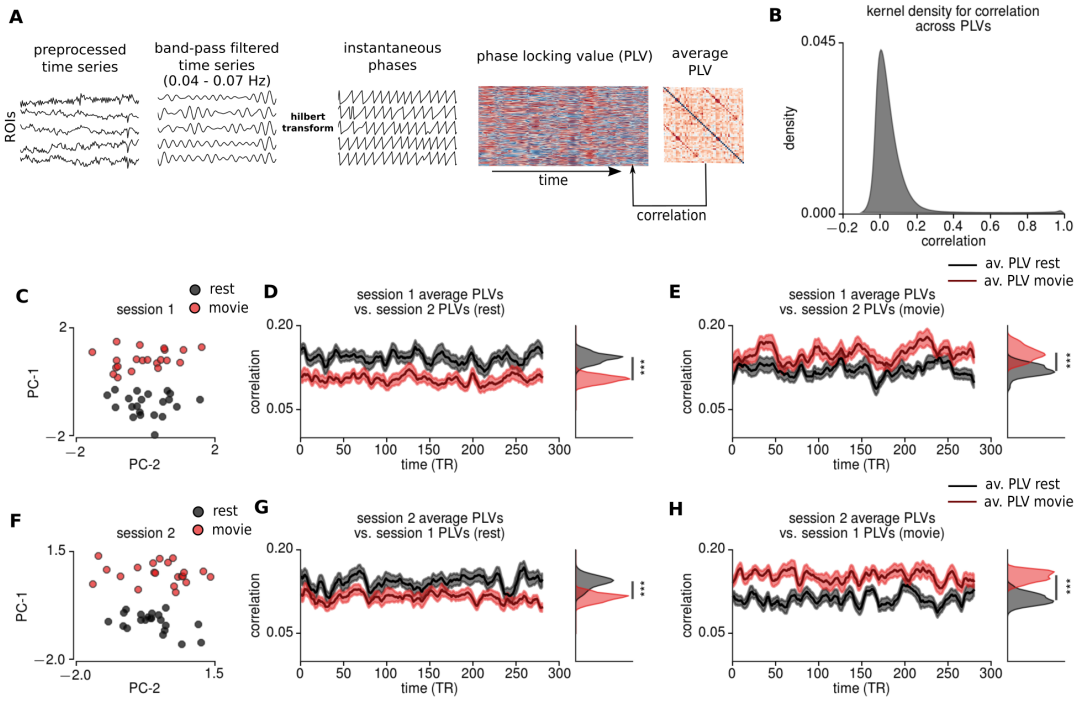

Figure 4. Stability of movie-specific components in dynamic FC. **A** The schematic describing the derivation of phase-locking value (PLV) dynamics. **B** Kernel density estimates of the correlations across PLVs. **C** Components projections of session 1. **D** Correlations between average PLVs at rest (black), during movie condition (red) and PLVs of resting state session 2. **E** Correlations between average PLVs at rest (black), during movie condition (red) and PLVs of movie session 2. **F-H** The same procedure as C-E, where the average PLVs were calculated for session 2 and projected on session 1 PLVs. The similarity between average resting-state PLVs and instantaneous PLVs of resting state sessions are significantly higher than those of movie sessions (Wilcoxon signed-rank test, p-value < 0.0001) **(D,G)**. Conversely, The similarity between average movie PLVs and instantaneous PLVs of movie sessions are significantly higher than those of resting state sessions (Wilcoxon signed-rank test, p-value < 0.0001) **(E,H)**. Shaded regions indicate standard error of mean. *** indicates p-values < 0.0001.

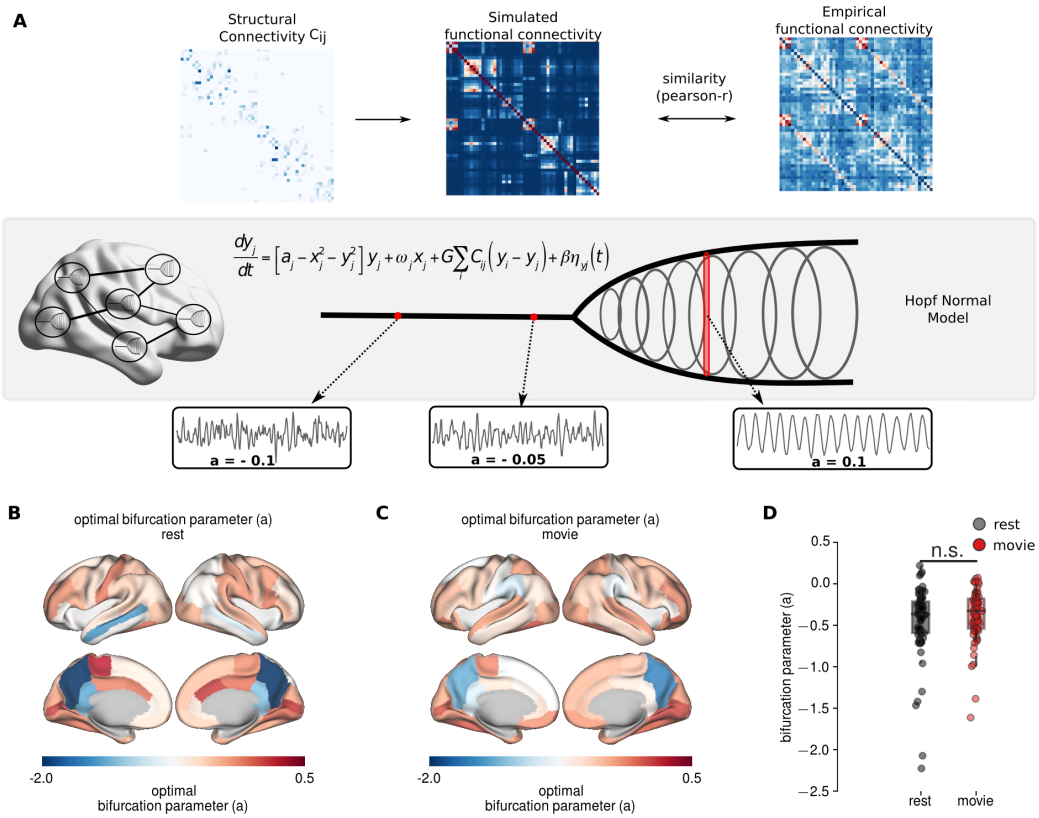

Figure 5. Large-scale computational modeling. **A** The schematic of the modeling framework. The BOLD activity of each region was described using Hopf normal model, where the local bifurcation parameters (a) mediate the local dynamics. Negative values of bifurcation parameter, a, indicates noise-driven activity, whereas positive values indicate oscillatory activity with increasing amplitude. Brain regions are coupled each other through DWI-derived SC matrix. The optimal model parameters were estimated using gradient descent optimization, which maximizes the similarity between empirical and model FC. **B** Mean optimal bifurcation parameter topography at resting state. **C** Mean optimal bifurcation parameter topography during movie condition. **D** The distributions of the bifurcation parameters during movie condition and resting state.

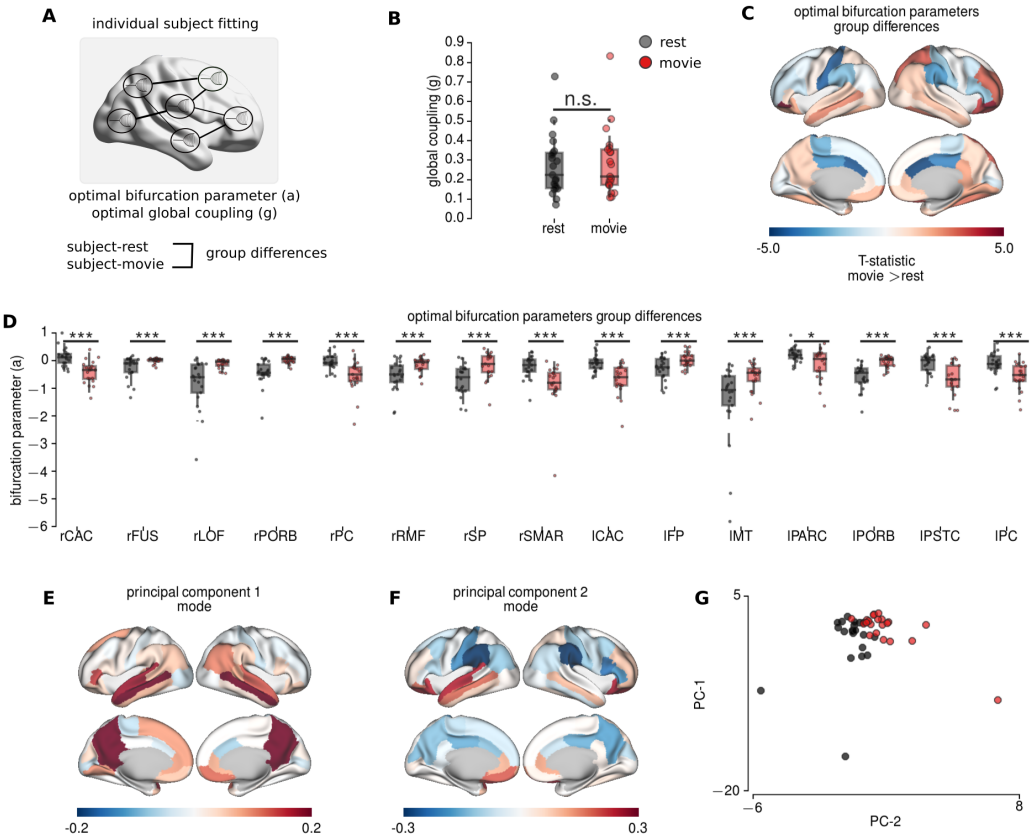

Figure 6. Modeling results for individual subject fitting. **A** The schematic of individual subject fitting. **B** The group differences for global coupling parameters did not show significant difference. **C-D** The group differences between optimal bifurcation parameters at rest (black) and during movie condition (red) (permutation t-test, 5000 permutations). **C** The topography of the group differences (T-statistics; hot colors indicate larger values during movie condition). **D** Boxplots of the regions showing significantly difference after FDR correction. **E-G** Principal component analysis applied to optimal bifurcation parameters in the model. **E** The topography of the first principal component. **F** The topography of the second principal component. PC-1 has higher values in precueus, posterior cingulate, medial temporal and frontal regions, exhibiting typical pattern associated to default mode network. PC-2 exhibit increased values in frontal and temporal regions, and decreased values particularly in supramarginal gyri and in medial brain regions. **G** The projections of the principal components on rest and movie sessions. *** indicate p-value < 0.0001.

Supplementary Figures

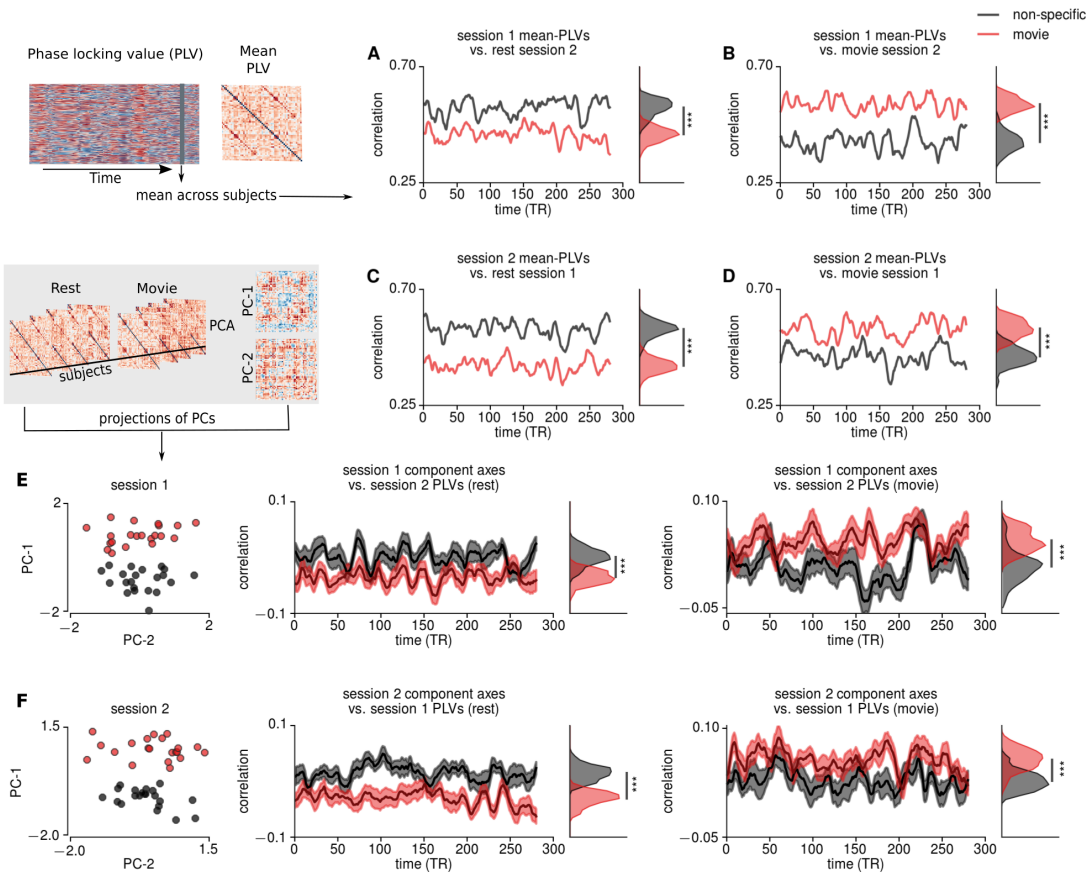

Supplementary Figure 1. A-D The similarity between mean PLVs and instantaneous PLVs of each condition. The mean-PLVs were computed for resting-state and movie sessions, and then the correlation coefficient between condition-specific mean-PLVs and instantaneous PLVs (averaged across subjects) were calculated. Since higher correlations are expected between average and instantaneous PLVs for the same sessions, the analyses were done cross-sessions: We calculated the correlation between mean-PLVs of rest/movie sessions 1 and instantaneous PLVs of rest/movie sessions 2, and vice versa. E-F The similarity between movie-specific and non-specific principal components and instantaneous PLVs.

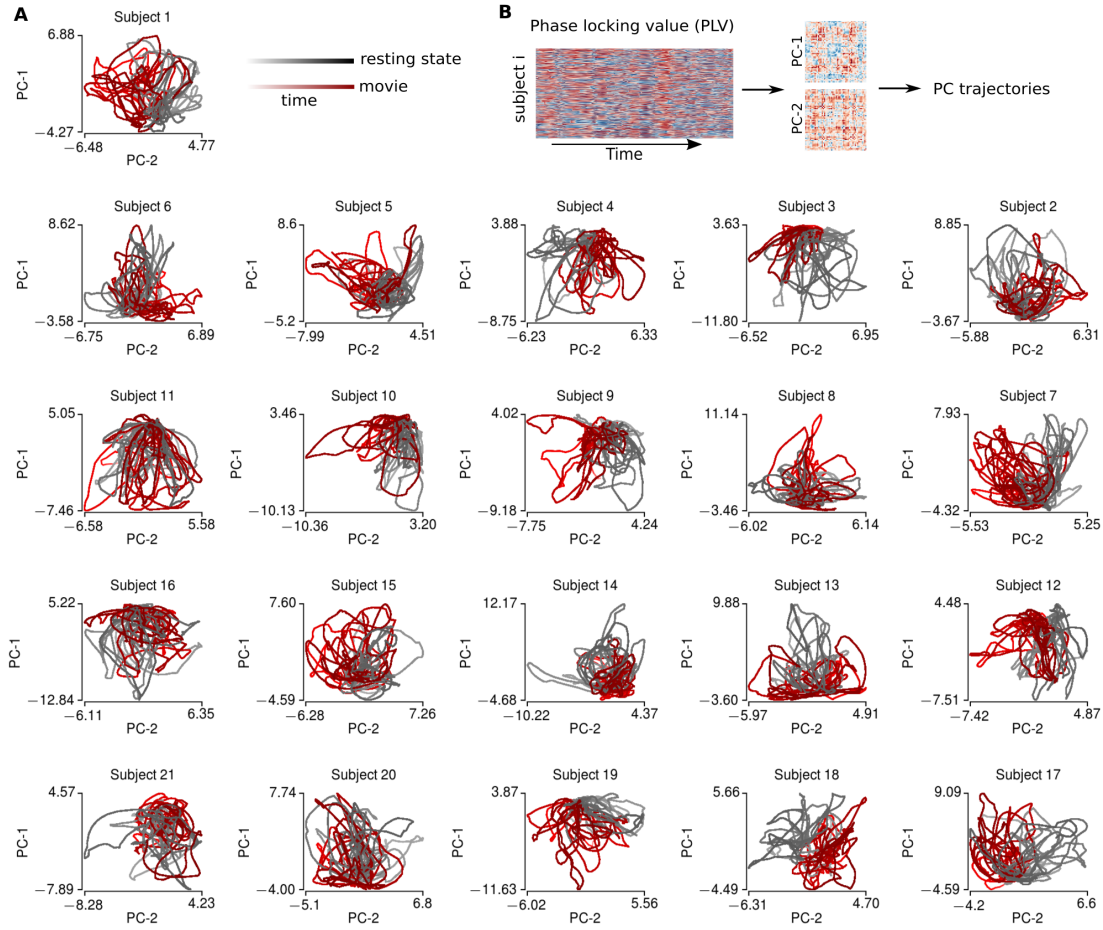

Supplementary Figure 2. The trajectories extracted from the PCA on dynamic functional connectivity of each subject. Gray colors indicate the time course of the components at rest, red colors indicate time course of the components while watching movie.

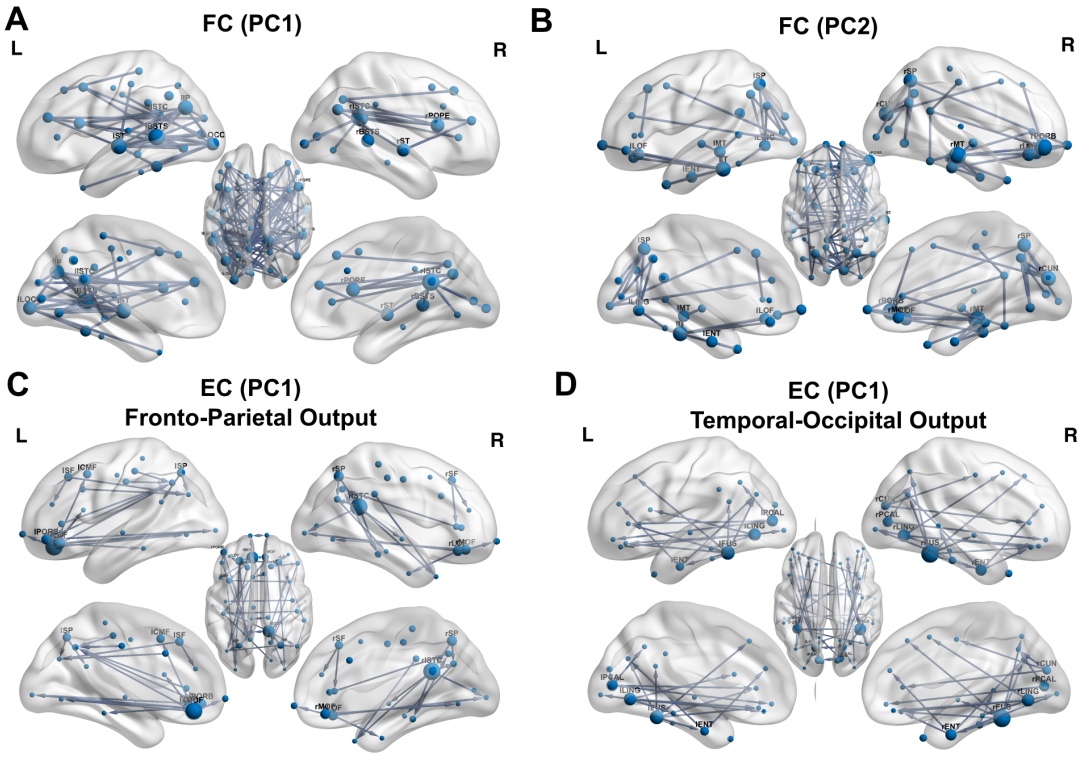

Supplementary Figure 3. The visualization of the highest 1% of the connections of PC-1 **(A)** and PC-2 **(B)** of FC, and PC-1 of EC **(C-D)**. **A** The non-specific component of FC exhibits larger connectivity strengths across posterior cingulate and precuneus, medial temporal and frontal regions as well as occipital cortex, which suggests default-mode network connectivity. **B** The movie-specific component of FC shows high connectivity between occipital and parietal regions, and between temporal and frontal regions. For effective connectivity (EC), movie-specific component reveals enhanced connectivity from frontal regions towards parietal and occipital brain regions **(C)**, and enhanced connectivity from occipital and temporal regions toward parietal and frontal regions **(D)**.

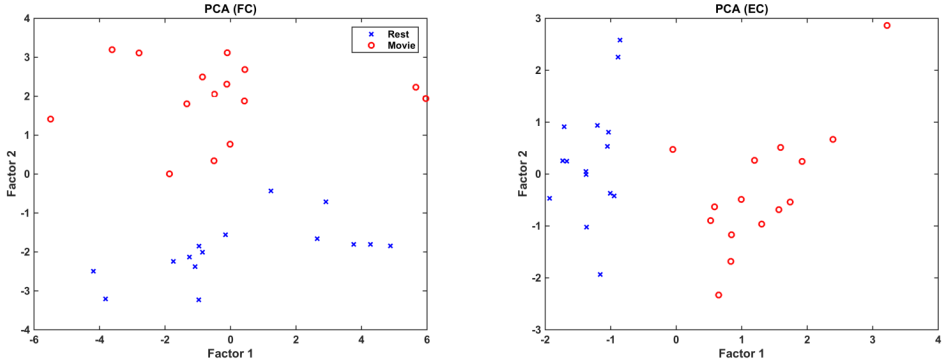

765

766 **Supplementary Figure 4.** The PCA on functional connectivity (left) and effective connectivity
767 (right). The separation between resting-state and movie conditions are clearer in EC.
768 Furthermore, there is a strong correlation between the projections of movie-specific and non-
769 specific components only for movie sessions for effective connectivity.

770